

## THE ULTRAVIOLET ABSORPTION SPECTRUM OF 3C 273<sup>1</sup>

J. N. BAHCALL,<sup>2</sup> B. T. JANNUZI,<sup>2</sup> AND D. P. SCHNEIDER  
 Institute for Advanced Study, School of Natural Sciences, Princeton, NJ 08540

G. F. HARTIG AND R. BOHLIN  
 Space Telescope Science Institute, 3700 San Martin Drive, Baltimore, MD 21218

AND

V. JUNKKARINEN  
 University of California, San Diego, La Jolla, CA 92093

Received 1991 April 1; accepted 1991 May 9

### ABSTRACT

We identify six Ly $\alpha$  absorption systems with equivalent widths greater than 0.2 Å in the ultraviolet spectrum of the nearby quasar 3C 273, more than expected on the basis of extrapolations of the observed number of Ly $\alpha$  clouds seen at large redshifts. Two Ly $\alpha$  lines appear to be produced by gas in the Virgo Cluster or by the halos of galaxies associated with the Virgo Cluster. We also detect all the interstellar absorption lines that are expected on the basis of abundance, atomic physics, and ionization considerations.

*Subject headings:* cosmology — quasars

### 1. INTRODUCTION

The quasar 3C 273 is the nearest ( $z_{\text{em}} = 0.158$ ) of the intrinsically bright quasars, with an apparent visual magnitude of  $V = 12.7$  at the time of our observations (Netzer & Mendelson 1991). We report here on high-resolution observations of 3C 273 in the ultraviolet, made as part of the science verification program of the *Hubble Space Telescope*. In § 2, we summarize the observations made with both *IUE* and with *HST* and in § 3 describe the measurement of the lines. In § 4, we identify the lines and indicate the implications of the identifications. We summarize our main scientific results in § 5.

### 2. OBSERVATIONS

We observed 3C 273 on 1991 January 14–16 with the Faint Object Spectrograph (FOS; see Ford 1985) using the three high-resolution ( $R = 1300$ ) gratings: G130H, G190H, and G270H. The spectra cover the region between 1150 and 3300 Å with a gap from 1600 to 1650 Å. Five apertures, including the  $0''.25 \times 2''.0$  slit, were used with each grating. Only the data obtained with the slit are discussed in this *Letter*; a future paper will compare and analyze the data from all the apertures.

Figure 1 shows the *HST*-calibrated data from all three gratings. The typical signal-to-noise ratio (SNR) is between 20 and 25 per pixel in the G130H data (2000 s exposure),  $\approx 30$  per pixel in the G190H data (1400 s exposure), and  $\approx 50$  per pixel in the best studied regions of the G270H data (1400 s exposure). The dispersions in the G130H, G190H, and G270H data are approximately 0.25, 0.36, and 0.52 Å pixel<sup>-1</sup>, respectively. The spectral resolutions (FWHMs) of the data are 1.1, 1.5, and 2.0 Å for the three gratings. The data from the blue

detector (G130H) were treated as a single 2000 s integration. Each 40 s integration with the red detector (G190H, G270H) was processed separately and then corrected for magnetic field effects with software developed by the FOS instrument team. We established the relative wavelength scale between different gratings by requiring that, in each grating, two to four strong ISM lines correspond to the same redshift and adjusted the absolute wavelength scale to be heliocentric using the geocoronal Ly $\alpha$  emission line.

Corrections for variations in sensitivity of the photocathodes and diodes were based upon observations of the white dwarf G191-B2B (WD 0501 + 5106). Since spectra shift on the photocathode due to magnetic field effects and the slight nonrepeatability of the positioning of the FOS filter-grating wheel, the wavelength offset was determined by cross-correlation. Residual errors in the flat-fielding dominate the statistical noise in some portions of the 3C 273 spectrum and create spurious weak features. We rejected narrow features that had similar strengths and shapes when observed through the slit and the  $4''.3$  aperture, since real lines have reduced resolution in the larger aperture. The flat-field structure is particularly strong in the central portion of the G190H spectrum, where variations exceed 3% in many pixels, but does not affect our measurements shortward of the Ly $\alpha$  emission line.

We also observed 3C 273 with the *International Ultraviolet Explorer* satellite on 1991 January 7, 13, 15–17, and 23 in order to set the zero point of the flux calibrations and to check upon possible variability. The *IUE* short-wavelength and long-wavelength cameras were used with the  $10'' \times 20''$  oval aperture to make low-resolution (7 Å) spectroscopic observations covering the wavelength region discussed in this *Letter*. Both the continuum and line emission were constant throughout the period of *IUE* observations to an accuracy of 10% or better.

### 3. MEASUREMENT OF ABSORPTION LINES

All features were fitted with single or multiple Gaussian profiles; line centers and equivalent widths (EWs) were determined using IRAF. Equivalent widths measured for the  $0''.3$  aperture

<sup>1</sup> Based on observations with the NASA/ESA *Hubble Space Telescope*, obtained at the Space Telescope Science Institute, which is operated by the Association of Universities for Research in Astronomy, Inc., under NASA contract NAS5-26555.

<sup>2</sup> Guest Observer with the *International Ultraviolet Explorer* satellite, which is sponsored and operated by the National Aeronautics and Space Administration, by the Science Research Council of the United Kingdom, and by the European Space Agency.

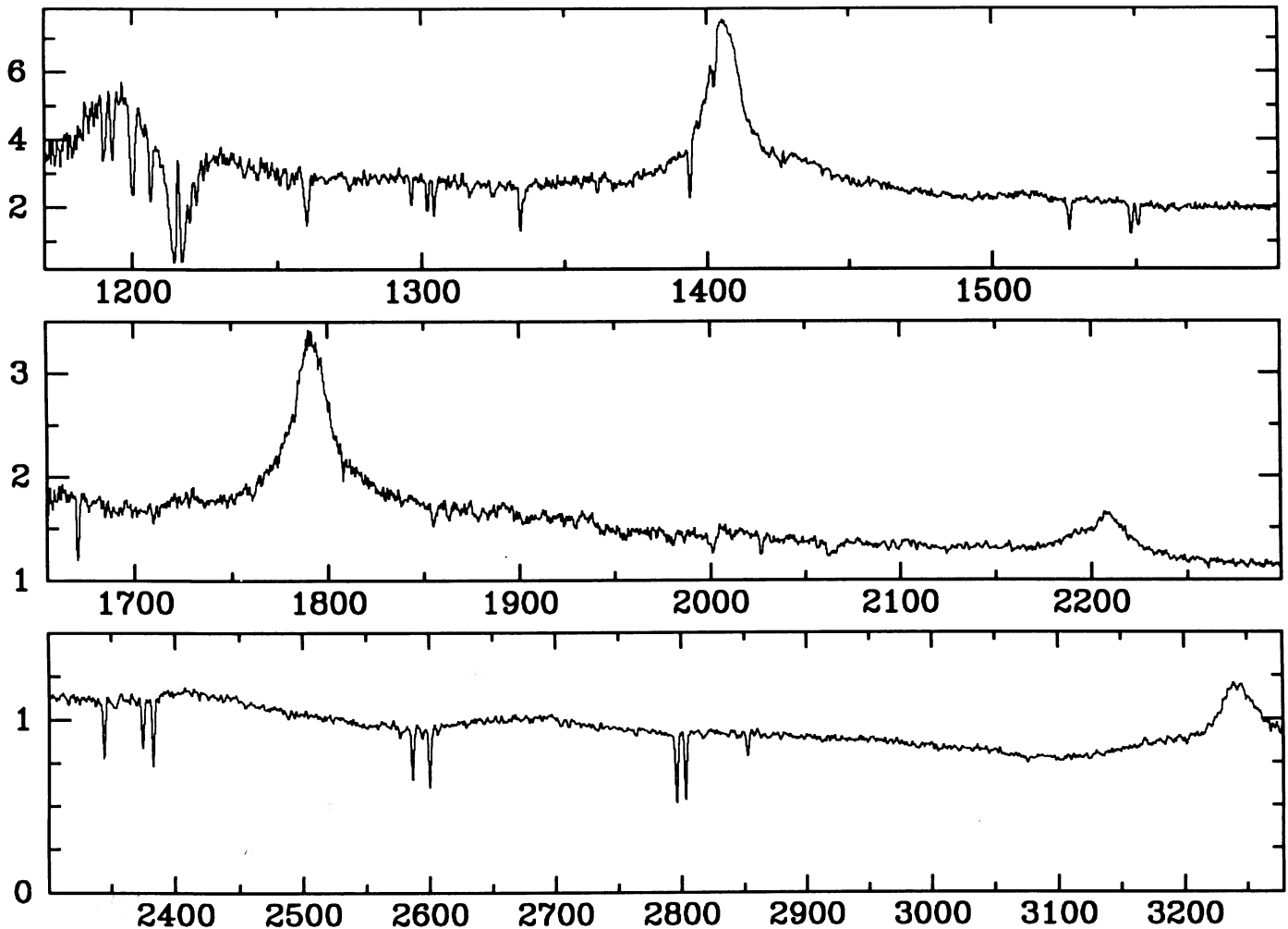


FIG. 1.—Faint Object Spectrograph spectrum of 3C 273 taken through the  $0'.25 \times 2'.0$  slit. The upper panel presents the data taken with the G130H grating (blue detector of the FOS); the middle and lower panels display the G190H and G270H data, respectively (red detector). The spectral resolutions (FWHMs) in the three spectra are  $1.1 \text{ \AA}$  (G130H),  $1.5 \text{ \AA}$  (G190H), and  $2.0 \text{ \AA}$  (G270H). The flux units are  $10^{-13} \text{ ergs s}^{-1} \text{ cm}^{-2} \text{ \AA}^{-1}$ .

and the slit agree within the measurement errors, calculated as in Young et al. (1979).

We measured all lines with an EW greater than a characteristic value of about  $0.1 \text{ \AA}$ . Candidate absorption lines were marked independently by J. N. B., B. T. J., and D. P. S. on plots of the calibrated flux versus wavelength. Even the weakest lines generally had a statistical significance in excess of  $3 \sigma$ . For inclusion in the complete sample, we required that all lines be  $3 \sigma$  detections with EWs greater than  $0.25 \text{ \AA}$  in the G130H and G190H data or greater than  $0.15 \text{ \AA}$  in the G270H data and that lines be consistent in the slit and the  $0'.3$  data. Table 1 lists the complete sample of 36 absorption lines. The columns contain (*left to right*) the measured line center, equivalent width, error in equivalent width, identification, vacuum wavelength of identification, difference between observed and laboratory wavelength, and comments.

#### 4. LINE IDENTIFICATIONS AND IMPLICATIONS

For identifications, we used a standard set of ultraviolet quasar absorption lines (Bahcall 1968, 1979) that correspond to the strongest allowed, one-electron, dipole transitions from

ground or excited fine-structure states of abundant elements.

##### 4.1. Galactic Gas

Table 1 shows the 28 identifications with interstellar lines of  $\text{Ly}\alpha$ , C II, C IV, N I, O I, Al II, Al III, Si II, Si III, Si IV, Mg I, Mg II, Fe II, and Mn II. The rms wavelength difference between the measured and the 28 standard lines is  $0.27 \text{ \AA}$ . The table also contains four identifications of interstellar lines that have equivalent widths too small to be included in the complete sample; the extra identifications include a transition originating on the excited fine structure state of C II, the resonant doublet of N V, and the weaker member of the Al III doublet. All lines that are expected to be present based upon abundance, atomic physics, and ionization considerations (Bahcall 1968, 1979) are identified in Table 1.

The column densities for the Galactic lines were calculated using the measurements given in Table 1. The data could not be satisfactorily represented on a curve of growth based on a single Gaussian velocity distribution; dividing the lines into high- and low-ionization species significantly improved the fits. The Doppler parameter ( $b = 2^{1/2}\sigma_v$ ) of the high-(low)-ioniza-

TABLE 1  
ULTRAVIOLET ABSORPTION LINES

$\lambda_{\text{obs}}$ (Å)	EW (Å)	$\sigma_{\text{EW}}$ (Å)	Identification Ion	$\lambda_0$	$\Delta\lambda$ (Å)	Comment
1190.44	0.463	0.111	Si II	1190.42	0.02	
1193.35	0.414	0.102	Si II	1193.28	0.07	
1200.22	0.982	0.085	N I	1199.90	0.32	
1206.44	0.553	0.078	Si III	1206.51	-0.07	
1215.7	7.0	1.5	Ly $\alpha$	1215.67	0.06	EW uncertain
1219.80	0.371	0.039	Ly $\alpha$			$cz = 1020 \text{ km s}^{-1}$
1222.12	0.414	0.092	Ly $\alpha$			$cz = 1590 \text{ km s}^{-1}$
1238.60	0.183	0.076	N V	1238.81	-0.21	NC
1243.04	0.178	0.101	N V	1242.80	0.24	NC
1260.08	0.789	0.057	Si II	1260.42	-0.34	+ SII (1259.53) ?
1275.23	0.251	0.059	Ly $\alpha$			$cz = 14,700 \text{ km s}^{-1}$
1296.52	0.287	0.057	Ly $\alpha$			$cz = 19,950 \text{ km s}^{-1}$
1302.08	0.372	0.050	O I	1302.17	-0.09	
1304.40	0.395	0.060	Si II	1304.37	0.03	
1317.08	0.292	0.096	Ly $\alpha$			$cz = 25,030 \text{ km s}^{-1}$
1325.10	0.238	0.057	Ly $\alpha$			$cz = 27,000 \text{ km s}^{-1}$ ; NC
1334.57	0.586	0.056	C II	1334.53	0.04	
1335.75	0.168	0.058	C II*	1335.70	0.05	NC
1361.53	0.146	0.072	Ly $\alpha$			$cz = 35,990 \text{ km s}^{-1}$ ; NC
1393.86	0.479	0.036	Si IV	1393.76	0.10	
1402.69	0.261	0.042	Si IV	1402.77	-0.08	
1526.77	0.477	0.047	Si II	1526.72	0.05	
1548.26	0.561	0.049	C IV	1548.20	0.06	
1550.75	0.402	0.050	C IV	1550.77	-0.02	
1670.92	0.534	0.036	Al II	1670.81	0.11	
1855.63	0.281	0.053	Al III	1854.72	0.91	
1862.95	0.182	0.049	Al III	1862.78	0.17	NC
1878.03	0.259	0.068				Broad; FF feature?
2026.55	0.266	0.035	Mg I	2026.47	0.08	
2065.09	0.440	0.061				
2344.16	0.727	0.031	Fe II	2344.21	-0.05	
2352.30	0.192	0.044				
2374.57	0.612	0.032	Fe II	2374.46	0.11	
2382.77	0.828	0.031	Fe II	2382.76	0.01	
2577.87	0.344	0.081	Mn II	2576.89	0.98	
2586.67	0.844	0.050	Fe II	2586.64	0.03	
2594.36	0.283	0.066	Mn II	2594.50	-0.14	
2600.25	0.980	0.051	Fe II	2600.18	0.07	
2606.71	0.155	0.026	Mn II	2606.47	0.24	
2796.27	1.098	0.025	Mg II	2796.35	-0.08	
2803.51	0.993	0.024	Mg II	2803.53	-0.02	
2852.85	0.392	0.027	Mg I	2852.97	-0.12	

NOTE.—NC = not in complete sample.

tion lines is  $63^{+60}_{-18}$  ( $15 \pm 1$ )  $\text{km s}^{-1}$ . The fit for the low-ionization features was not as good as that for the high-ionization lines. The column densities for the damped Ly $\alpha$ , high-ionization, and low-ionization lines are, respectively,  $\log N_{\text{col}} \approx 20, 13.5\text{--}14$ , and  $13.5\text{--}17$ .

Absorption is detected from the excited fine-structure state of C II, but not from the excited fine-structure state of Si II. The C II excited fine-structure absorption is most likely produced in an H I region and corresponds (see Bahcall & Wolf 1968) to a neutral hydrogen density of order  $n_{\text{H}} \sim 10^3$  ( $N_{\text{ex}}/N_{\text{ground}}$ )  $\text{cm}^{-3}$ , where ( $N_{\text{ex}}/N_{\text{ground}}$ ) is the ratio of excited to ground-state populations. The Si II absorption is presumably produced in an H II region, and the absence of transitions originating on excited fine-structure states sets a limit in this region on the ambient electron density of (Bahcall & Wolf 1968)  $n_e \lesssim 10^3$  ( $N_{\text{ex}}/N_{\text{ground}}$ )  $\text{cm}^{-3}$ .

#### 4.2. Ly $\alpha$ Clouds

Ly $\alpha$  absorption at small redshifts apparently produces five of the eight lines in the complete sample that are not identified

with Galactic absorption. The total range over which we have good observations exceeds  $1770 \text{ \AA}$ . If the eight unidentified lines were uniformly sprinkled over this entire range, then the Poisson probability would be 0.2% that five of eight lines were crowded, as observed, into the  $192 \text{ \AA}$  between the rest wavelength of Ly $\alpha$  and the redshifted Ly $\alpha$  emission line. One of the remaining two lines may be a flat-field artifact ( $1878.03 \text{ \AA}$ ). In addition, there are two other real lines that are apparently Ly $\alpha$  absorption systems but which have EWs too small to be in the complete sample. These lines, at  $1325.10 \text{ \AA}$  (EW =  $0.24 \text{ \AA}$ ) and  $1361.53 \text{ \AA}$  (EW) =  $0.15 \text{ \AA}$ , are included in Table 1.

The Ly $\alpha$  systems have H I column densities of  $14 \lesssim \log N_{\text{col}} \lesssim 16$  for  $b \approx 35 \text{ km s}^{-1}$ . The maximum EW that any line could have and not be in the complete sample ( $0.25 \text{ \AA}$ ) limits the amount of metals present in the clouds to  $\log N_{\text{col}} \lesssim 15$ . The absence in our spectra of metal lines from the Ly $\alpha$  systems (hereafter called clouds) is not surprising; we would not expect to detect the metal lines unless the hydrogen is highly ionized.

The Ly $\alpha$  lines at  $1219.8 \text{ \AA}$  and  $1222.1 \text{ \AA}$  are probably caused by gas in the Virgo Cluster or in halos of galaxies associated with the Virgo Cluster. The heliocentric velocities of the two Ly $\alpha$  systems are  $1020 \pm 17 \text{ km s}^{-1}$  and  $1591 \pm 45 \text{ km s}^{-1}$ . The Virgo Cluster has an average velocity of  $1158 \text{ km s}^{-1}$  (Huchra 1985) and contains galaxies with a broad range of velocities that bracket the two Virgo Ly $\alpha$  clouds. The large gas cloud H1 1225+01 discovered by Giovanelli & Haynes (1989) has a systemic velocity of  $1275 \text{ km s}^{-1}$  and may well be associated with the Virgo Cluster. The center of H1 1225+01 is located about  $250 \text{ kpc} \times d(\text{H1 1225+01})/20 \text{ Mpc}$  from the line of sight to 3C 273 and could be the source of one or more of the Virgo Ly $\alpha$  absorption lines. Some Ly $\alpha$  systems may be caused (Bahcall 1979) by large gas clouds or halos surrounding galaxies that contain primarily hydrogen and helium, a suggestion that is more plausible in the case of a nascent galaxy like H1 1225+01. Figure 2 shows the spectrum in the region between  $1210 \text{ \AA}$  and  $1225 \text{ \AA}$ .

Using the conventional parameterization (Sargent et al. 1980; Murdoch et al. 1986; Lu, Wolfe, & Turnshek 1991), the expected number,  $N$ , of Ly $\alpha$  clouds in the spectrum of a nearby quasar may be written

$$N(z_{\text{em}}, W > W_{\text{cutoff}}) = A_0(1 + \gamma)^{-1} \times [(1 + z_{\text{em}})^{\gamma+1} - 1] \exp \left[ -\left( \frac{W_{\text{cutoff}}}{0.3 \text{ \AA}} \right) \right], \quad (1)$$

where  $W_{\text{cutoff}}$  is the minimum considered rest equivalent width. The values of  $A_0$  that are determined by extrapolating large redshift observations are uncertain, but have been estimated recently by Murdoch et al. (1986) and by Lu et al. (1991). The line of sight to 3C 273 contains six Ly $\alpha$  systems with EWs above  $0.20 \text{ \AA}$ , a lower limit frequently adopted in discussions in the literature. The observed number of lines is 5 times larger than predicted by the parameters determined by Murdoch et al. and is 10 times larger than predicted by the parameters of Lu et al. Even ignoring the two lines that apparently arise from the Virgo Cluster, the number of observed Ly $\alpha$  systems is larger than expected at the 90% confidence level.

The effects of cosmological evolution are evident in the qualitative appearance of the absorption-line spectrum of 3C

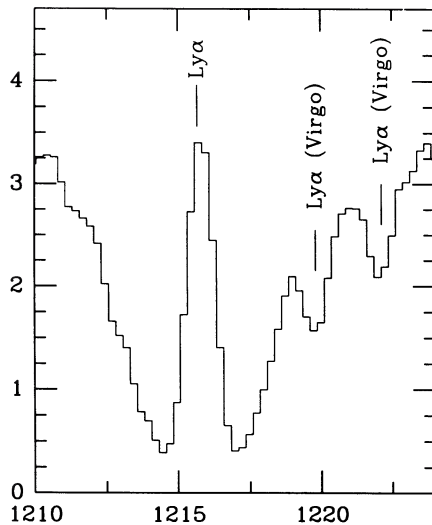


FIG. 2.—The region between 1210 and 1225 Å in the slit spectrum. The resolution is  $\approx 1.1$  Å. The most prominent feature is the strong Galactic Ly $\alpha$  absorption line. The geocoronal Ly $\alpha$  emission line is seen in the center of the Galactic absorption line. The two marked absorption features located on the red shoulder of the Galactic Ly $\alpha$  line are probably produced by gas in the Virgo Cluster or by halos of galaxies associated with the Virgo Cluster. The flux units are  $10^{-13}$  ergs  $s^{-1}$   $cm^{-2}$  Å $^{-1}$ .

273 (see Fig. 1). The familiar Ly $\alpha$  forest (Lynds 1971), which dominates the spectra of large-redshift quasars shortward of the Ly $\alpha$  emission line, is missing from Figure 1. Instead of having about one strong Ly $\alpha$  system every few Å, as is characteristic of large-redshift quasars, Figure 1 and Table 1 exhibit

only about one strong Ly $\alpha$  absorption system every 50 or 100 Å (depending upon the EW threshold).

#### 5. SUMMARY AND DISCUSSION

We find in the direction of 3C 273 two Ly $\alpha$  absorption systems that are probably associated with the Virgo Cluster, an unexpectedly large total number of Ly $\alpha$  systems, and a rich spectrum of Galactic absorption lines. The expected number of heavy element absorption systems is  $\sim (3-8)z_{em}$  (Bahcall & Spitzer 1969; Sargent, Boksenberg, & Steidel 1988), which is consistent with none being observed. The depression of the continuum below the Ly $\alpha$  emission line is  $\tau = 0.04^{+0.06}_{-0.04}$ , where systematic uncertainties in the flat field, photometric calibrations, and intrinsic spectrum of the quasar dominate the errors. This depression corresponds to a limit (Gunn & Peterson 1965) on the uniformly distributed neutral hydrogen of  $n_H(z \sim 0.1) < 3 \times 10^{-12} h_{100} \text{ cm}^{-3}$ .

The OSS personnel at the Space Telescope Science Institute provided expert help with the data acquisition; Y. Kondo made available director's discretionary time on *IUE* for the crucial simultaneous observations; and the operations and scientific staff of *IUE*, especially J. Bonnell, provided valuable assistance. B. Bhattacharya assisted with the reduction of the FOS spectra. The FOS instrument definition team, most notably E. A. Beaver and R. Lyons at UCSD, developed the software correction for the image motion induced by Earth's magnetic field. We appreciate valuable discussions with B. Draine, U. Feldman, E. Jenkins, H. Netzer, W. L. W. Sargent, L. Spitzer, C. Steidel, and B. Yanny. This work was supported in part by NASA contract NAS5-29225 and STScI grant GO-2424.01.

#### REFERENCES

- Bahcall, J. N. 1968, *ApJ*, 153, 679  
 ———. 1979, in *IAU Colloquium 54, Scientific Research with the Space Telescope*, ed. M. S. Longair & J. W. Warner (NASA CP-2111), 215  
 Bahcall, J. N., & Spitzer, L. 1969, *ApJ*, 156, L63  
 Bahcall, J. N., & Wolf, R. A. 1968, *ApJ*, 152, 701  
 Ford, H. C. 1985, *Faint Object Spectrograph Instrument Handbook* (Baltimore: Space Telescope Science Institute)  
 Giovanelli, R., & Haynes, M. P. 1989, *ApJ*, 346, L5  
 Gunn, J. E., & Peterson, B. A. 1965, *ApJ*, 142, 1633  
 Huchra, J. P. 1985, in *The Virgo Cluster of Galaxies*, ed. O.-G. Richter & B. Binggeli (Garching: European Southern Observatory), 181  
 Lu, L., Wolfe, A. M., & Turnshek, D. A. 1991, *ApJ*, 367, 19  
 Lynds, C. R. 1971, *ApJ*, 164, L73  
 Murdoch, H. S., Hunstead, R. W., Pettini, M., & Blades, J. C. 1986, *ApJ* 309, 19  
 Netzer, H., & Mendelson, H. 1991, private communication  
 Sargent, W. L. W., Boksenberg, A., & Steidel, C. C. 1988, *ApJS*, 68, 539  
 Sargent, W. L. W., Young, P. J., Boksenberg, A., & Tytler, D. 1980, *ApJS*, 42, 41  
 Young, P. J., Sargent, W. L. W., Boksenberg, A., Carswell, R. F., & Whelan, J. A. J. 1979, *ApJ*, 229, 891